

Crown ether-cycloparaphenylene hybrid multimacrocycles: Insights into supramolecular gas sensing and biological potential

Yaning Hu,¹ Tong Li,^{2,3} Taotao Su,¹ Wudi Shi,¹ Yabing Yu,¹ Beibei Li,¹ Menghua Li,¹ Sheng Zhang,¹ Yuan-Qing Xu,¹ Qi Liu,^{*,1} Di Wu,^{*,2} Youzhi Xu^{*,1}

¹College of Chemistry and Molecular Sciences, Henan University, Kaifeng 475004, P. R. China. E-mail: qiliu@henu.edu.cn; youzhixu@henu.edu.cn

²School of Public Health, Zhengzhou University, Zhengzhou 450001, P. R. China. E-mail: wudi22@zzu.edu.cn

³School of Chemistry, Zhengzhou University, Zhengzhou 450001, P. R. China.

Abstract: The topologically intriguing multimacrocyclic architecture is endowed with distinct physical and chemical properties. The synthesis of hybrid macrocycles combining crown ethers and cycloparaphenylenes (CPPs) presents a promising strategy for developing multifunctional supramolecular systems. Herein, we first report the precise construction of a series of crown ether-CPP hybrid multimacrocycles with enhanced photophysical properties and diverse host-guest interactions. Notably, the trimacrocyclic hybrid adopts a molecular tweezer-like conformation, resulting in a significantly higher fullerene binding affinity compared to the bismacrocyclic. The fullerene complex showed improved conductivity and sensitivity with a limit of detection (LOD) of 19 ppb for NO₂ with excellent cyclic stability and reliable. Additionally, the bismacrocyclic exhibits significant cytotoxicity against cancer cell lines at low concentrations and enables fluorescence-based detection of inflammatory responses, highlighting its potential for biosensing applications. These findings underscore the versatility of crown ether-CPP hybrid macrocycles in supramolecular sensing and biochemistry, offering new avenues for the design of functional nanomaterials.

Introduction

In the realm of supramolecular chemistry, the synthesis and exploration of innovative macrocycles play a pivotal role in advancing materials suitable for applications in drug delivery, catalysis, sensing, and various other fields.¹ Cycloparaphenylenes (CPPs) represent a unique class of π -conjugated macrocycles, distinguished by their strained structure and size-dependent chemical² and photophysical properties³. These intriguing molecules have attracted

considerable attention from researchers in the fields of chemistry and materials science.⁴ Recent studies have highlighted the fascinating properties of topologically unique multi-macrocycles, which exhibit behavior distinct from that of monocyclic structures (Fig. 1a).⁵ For instance, Du et al. reported CPP-based bismacrocycles that exhibit dual-emission behavior, characterized by tunable aggregation-induced emission and enhanced chiroptical properties.⁶ Similarly, Yam and Jiang have independently synthesized rigid and heterotopic bismacrocycles combining CPP and pillar[5]arene, showcasing remarkable luminescent and host-guest recognition properties (Fig. 1b).⁷

Crown ethers as an intriguing class of macrocycles with flexible skeleton, renowned for their ability to selectively bind metal cations through coordination interactions and adeptly fabricate mechanically interlocked molecules (MIMs) via hydrogen bonding.⁸ This synergy of properties offers exciting opportunities for innovative molecular designs. For example, we recently have reported the synthesis of a rare hetero[3]catenane using a ring-in-ring assembly strategy, incorporating unaltered [12]CPP, 24-crown-8 and a dibenzylammonium macrocycle (Fig. 1b).⁹ To further explore the potential of the hybrids of CPPs and crown ethers. Herein, we present the synthesis of hybrid bis- and trimacrocycles combining CPPs and crown ethers. We then investigated their supramolecular properties and the application in organic electronic devices. Additionally, we conducted cell imaging and in vitro antitumor activity studies to evaluate their potential for biological applications.

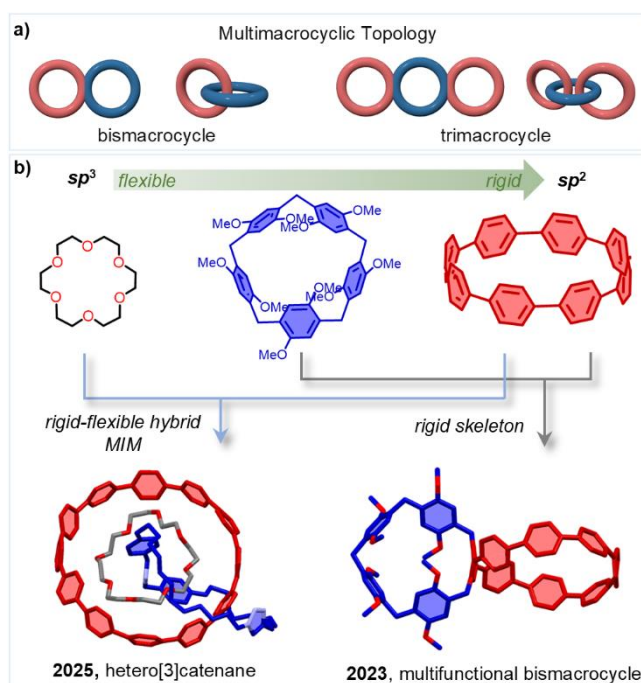


Fig. 1 | a) Illustration of two types of multimacrocylic topology. b) Selected examples of CPP-hybrid multimacrocycles.

Result

Synthesis and Characterization. The pivotal intermediates for the synthesis of bis- and trimacrocycles are outlined in Fig. 2a. The hoop-shaped multimacrocycles **5–7**, varying in diameter, were successfully synthesized via Suzuki–Miyaura cross-coupling ([dppf Pd G4], K₃PO₄, 1,4-dioxane–H₂O, 85 °C, 24 h) between iodinated dibenzo-crown ethers **1–2** and diboronate **4**, followed by reductive aromatization (sodium naphthalenide, THF, –78 °C, 2 h). The [8]CPP-based bismacrocycles **5** and **6**, incorporating 18-crown-6 and 24-crown-8, were obtained in with two-step yield of of 20% and 17%, respectively. Notably, the reaction between iodinated dibenzo-crown ethers **3** and diboronate **4** is theoretically expected to yield both the [8]CPP-based trimacrocycle **7** and the [16]CPP-based alternative topological multimacrocycle **8**. However, after separation and purification, combined with NMR and emission spectroscopy analysis, only the 24-crown-8-bridged trimacrocycle **7** was successfully synthesized, with a two-step yield of 10%. This outcome is presumably due to the mismatch between the torsional angle of substrate **4** and the size of **3**, which hinders the formation of the alternative multimacrocycle.^[10]

These multimacrocycles were fully characterized by NMR spectroscopy and high-resolution mass spectrometry (HRMS) after standard workup and purification. The crown ether units within the macrocyclic backbone facilitated clear detection of sodium and potassium ion association in the mass spectra (Fig. 2b). Compared to bismacrocycle **6**, trimacrocycle **7** features two identical [8]CPP units flanking the dibenzo-24-crown-8 core, enhancing molecular symmetry, as confirmed by its ¹H NMR spectrum (Fig. 2c, Fig. S1).

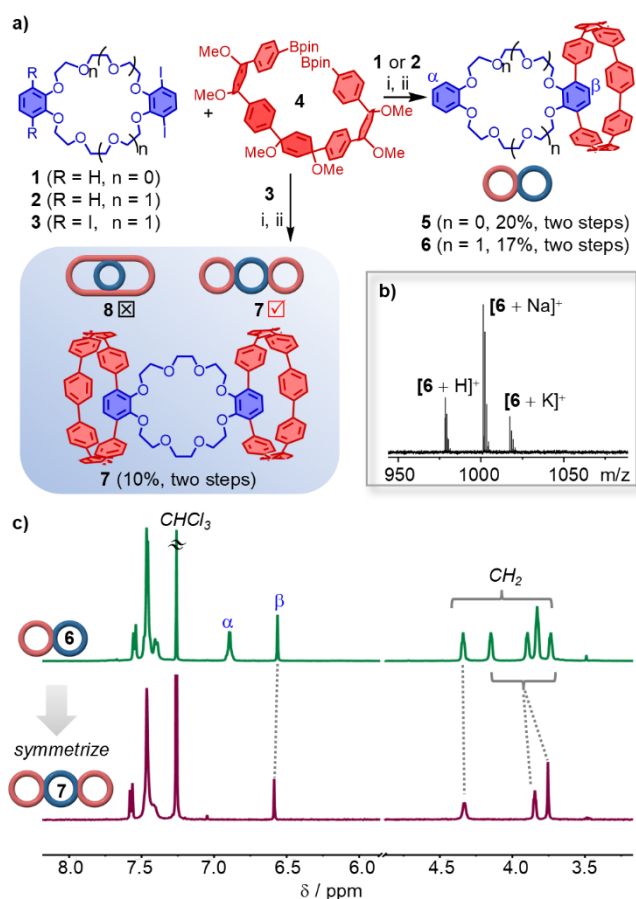


Fig. 2 | Synthesis of crown ether-cycloparaphenylene hybrids. a) represent the key synthetic procedures. Reaction conditions: i) [dppf Pd G₄], K₃PO₄, 1,4-dioxane–H₂O, 85 °C, 24 h. ii) sodium naphthalenide, THF, –78 °C, 2 h. b) The HRMS-ESI of **6**. c) Partial ¹H NMR spectra (CDCl₃, 298 K, 500 MHz) of **6** and **7**.

Single crystals of **6** were prepared by slow diffusion of diisopropyl ether into toluene solution. As shown in Fig. 3 (left), the structure of **6** can be recognized as an integration of the two classic macrocycles, dibenzo-24-crown-8 and [8]CPP. The two independent cavities do not overlap with each other, the distance between the two phenyl rings of dibenzo-24-crown-8 and the diameter of [8]CPP are calculated to be 10.5 Å and 10.4 Å, respectively. Then, we dissolved equimolar amounts of compounds **6** and KPF₆ in a 1:1 CHCl₃–MeOH solution and obtained single crystals of the metal complex **6**⊃K⁺ through slow evaporation of the CHCl₃. Analyzing the X-ray crystal structure of complex **6**⊃K⁺, we can see that the 24-crown-8 ring tightly encapsulates the potassium ion by folding, primarily via multiple electrostatic interactions, the average distance of O⋯K is 2.5 Å (Fig. 3, right). Due to the introduction of the 24-crown-8 ring, [8]CPP no longer presents ordered columnar packing,¹¹ but a random packing with no apparent supramolecular interactions between the complex molecules was found in the solid state (Fig. S2 and S3). This also leads to **6** having better solubility in organic solvents.

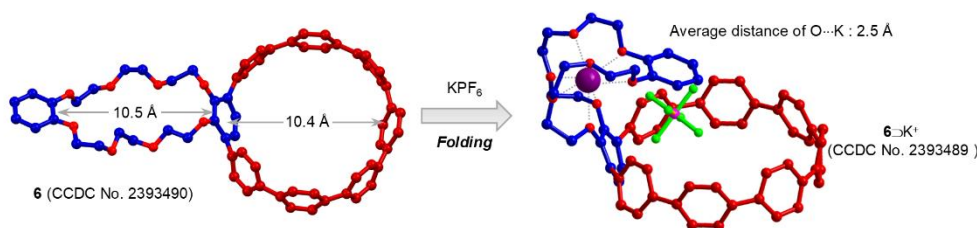


Fig. 3 | X-ray crystal structure of **6** and the complex of $6 \cdot K^+$.

Photophysical Properties. The absorption spectra of multimacrocycles **6** and **7** closely resemble that of [8]CPP, exhibiting a primary absorption maximum around 335 nm and a shoulder near 400 nm, attributed to the HOMO \rightarrow LUMO transition. The molar extinction coefficient (ϵ) at 335 nm for **6** ($8.5 \times 10^4 \text{ M}^{-1} \text{ cm}^{-1}$) is comparable to that of [8]CPP, whereas **7** ($1.3 \times 10^5 \text{ M}^{-1} \text{ cm}^{-1}$) exhibits approximately 1.5 times higher absorption. This increase suggests that the two CPP units in **7** behave as independent chromophores, consistent with Beer's Law, although possible excitonic coupling effects cannot be ruled out.

In dichloromethane at 298 K, **6** and **7** display fluorescence emission bands centered at 525 nm and 530 nm, respectively, upon excitation at 340 nm (Fig. 4a). Compared to [8]CPP, these multimacrocycles exhibit a slight blue shift, which may arise from subtle structural distortions induced by the crown ether ring. Such distortions could slightly reduce effective π -conjugation, thereby increasing the energy gap between the excited and ground states. More notably, their fluorescence quantum yields ($\Phi_F = 0.58$ for **6**, 0.60 for **7**) are significantly higher than that of [8]CPP ($\Phi_F = 0.10$)³, indicating a strong enhancement in radiative emission efficiency. The fluorescence enhancement can be attributed to multiple factors. First, orbital symmetry breaking in the CPP backbone may increase the transition dipole moment, thereby enhancing radiative decay rates (Fig. 4b).¹² Second, the introduction of crown ether moieties may impose structural rigidity, reducing non-radiative relaxation pathways such as intramolecular rotations or vibrations. Time-resolved fluorescence measurements reveal that the fluorescence lifetimes of **6** (2.8 ns) and **7** (4.3 ns) are comparable to that of [8]CPP, suggesting that the increased fluorescence quantum yield is primarily due to suppression of non-radiative decay rather than an intrinsic increase in excited-state lifetime. In the solid state, **6** and **7** maintain Φ_F values of 14% and 18%, respectively, despite the potential for aggregation-caused quenching (ACQ). This suggests that the presence of crown ether substituents helps mitigate intermolecular π - π stacking, likely by introducing steric hindrance and restricting molecular aggregation.

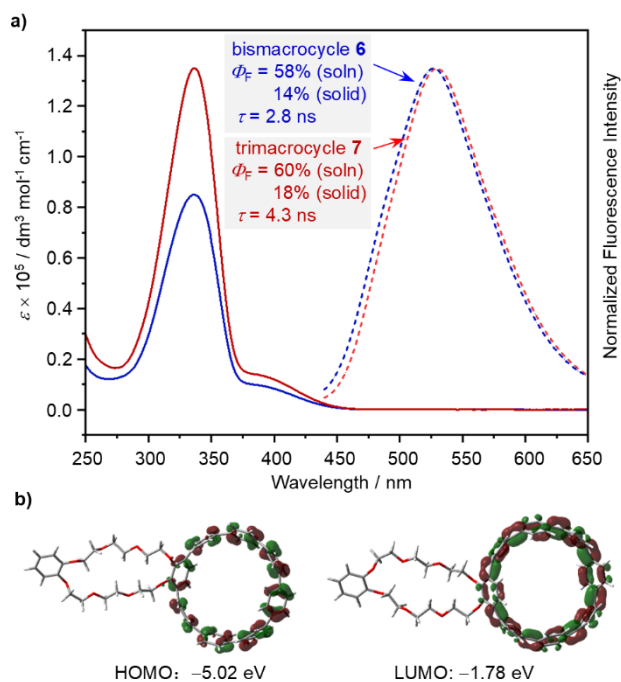


Fig. 4 | a) UV-Vis absorbance (solid lines) and fluorescence (dashed lines) spectra for **6** and **7** (conc. 5.0×10^{-6} M in dichloromethane). b) Frontier molecular orbitals of **6** calculated at the B3LYP/6-31G(d) level of theory (isovalue 0.03).

Guest Recognition and Gas Sensing. Analysis of the X-ray crystal structure of **6** revealed that the flexible crown ether backbone adopts a folded conformation. This structural feature led us to hypothesize that trimacrocycle **7** might serve as an effective host for fullerene recognition.¹² While [10]CPP is well known for encapsulating C_{60} via strong π - π interactions, the smaller size of [8]CPP generally results in weaker binding. Given the structural modifications introduced in **7**, we sought to evaluate its binding properties toward C_{60} through fluorescence quenching titrations in toluene.

The binding study revealed that $\mathbf{6} \supset C_{60}$ forms with an association constant ($K_A = (1.5 \pm 0.05) \times 10^5 \text{ M}^{-1}$, Fig. S4), which is significantly lower than $[10]\text{CPP} \supset C_{60}$ ($3.6 \times 10^6 \text{ M}^{-1}$)¹⁴ but higher than unmodified [8]CPP, likely due to additional dispersion interactions introduced by the crown ether side chains. In contrast, titration experiments between **7** and C_{60} exhibited a 1:1 (host : guest) binding equilibrium, with a much higher association constant ($K_{1:1} = (2.4 \pm 0.5) \times 10^6 \text{ M}^{-1}$) compared to $\mathbf{6} \supset C_{60}$.¹⁵ This suggests that **7** adopts a molecular tweezer-like conformation,¹⁶ where its two CPP units cooperatively encapsulate the fullerene, significantly enhancing its binding affinity. DFT-optimized structures confirm that C_{60} sits symmetrically within the cavity of **7**, stabilized primarily by dispersion forces between the π -conjugated CPP units and the fullerene surface (Fig. S5, Table S3). Independent Gradient Model (IGM) analysis further highlights strong non-covalent interactions in the $\mathbf{7} \supset C_{60}$ complex, reinforcing the

enhanced binding affinity observed experimentally.

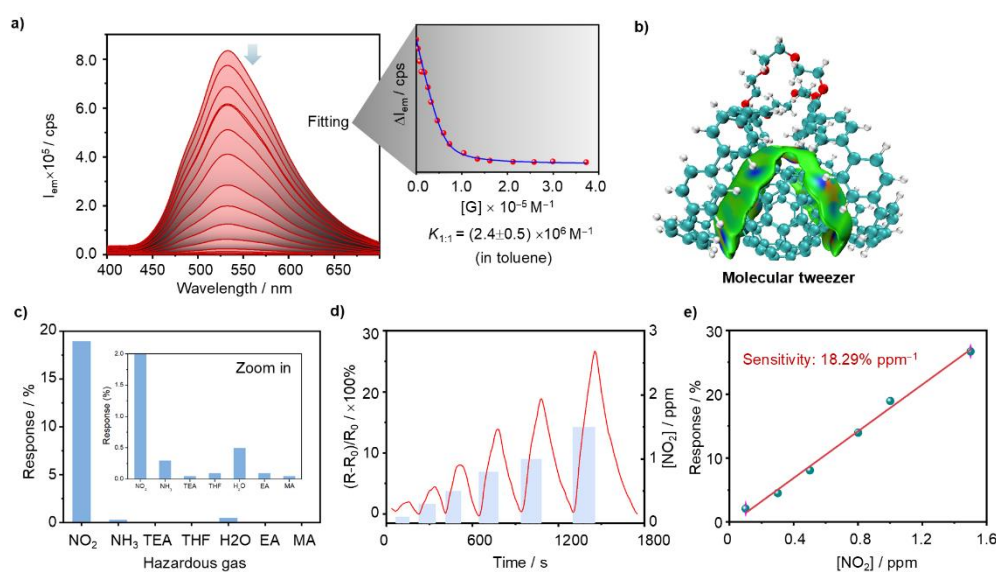


Fig. 5 | a) Fluorescence titrations between **7** (conc. $6.0 \times 10^{-6} \text{ M}^{-1}$) and C_{60} in toluene. Association constants were obtained by fitting the data according to a 1:1 (host : guest) stoichiometric model. b) IGM analyses of the complex of $7 \supset \text{C}_{60}$ ($\delta g_{\text{inter}} = 0.003$). c) Response of $7 \supset \text{C}_{60}$ for different hazardous gas. d) Dynamic response curves of $7 \supset \text{C}_{60}$ toward 0.1–1.5 ppm NO_2 . e) The possible sensing mechanism of $7 \supset \text{C}_{60}$ for NO_2 .

The interactions and photophysical properties of CPP and C_{60} have been extensively studied.^{13a} However, their potential applications in semiconductor devices remain underexplored. Therefore, we further investigated the use of CPP and its fullerene complexes in organic electronic devices. Thin film electrodes were fabricated on interdigital electrodes (IDEs) using the quasi-Langmuir–Shäfer (QLS) technique, which were then employed as chemiresistive gas sensors (CGS) for detecting hazardous gases.¹⁶ The conductivity characteristics of **7** and the $7 \supset \text{C}_{60}$ complex were initially assessed through I – V curves (Fig. S7). Due to the incorporation of an electron transport mediator and the push-pull electronic effects between C_{60} and **7**, the $7 \supset \text{C}_{60}$ complex demonstrated significantly enhanced conductivity ($6.37 \times 10^{-7} \text{ S cm}^{-1}$) compared to **7** alone, making it more suitable for CGS applications.

We applied the $7 \supset \text{C}_{60}$ -based chemiresistive sensor for detecting a variety of hazardous gases and volatile organic compounds (VOCs). As shown in Fig. 5c, the $7 \supset \text{C}_{60}$ complex exhibited a markedly higher response to NO_2 than to other test gases, highlighting its exceptional specificity toward NO_2 . Subsequently, we examined the sensitivity of both $7 \supset \text{C}_{60}$ and **7** to NO_2 in the concentration range of 0.1–1.5 ppm. As illustrated in Fig. 5d and Fig. S8, the $7 \supset \text{C}_{60}$ complex displayed superior response and recovery characteristics to NO_2 in this concentration

range, attributable to its enhanced conductivity and the presence of the donor-acceptor (D-A) structure. Furthermore, as depicted in Fig. 5e, the $7\supset C_{60}$ complex exhibited a strong linear relationship with NO_2 concentrations from 0.1 to 1.5 ppm, with a sensitivity of $18.29\% \text{ ppm}^{-1}$. Based on this, the limit of detection (LOD) for NO_2 was calculated to be 19 ppb, indicating the sensor's potential for practical applications. Additionally, the cyclic stability of the $7\supset C_{60}$ complex at 1 ppm NO_2 was evaluated, with results showing a coefficient of variation not exceeding 1.2%, demonstrating the excellent cyclic stability of the $7\supset C_{60}$ -based sensor (Fig. S9).

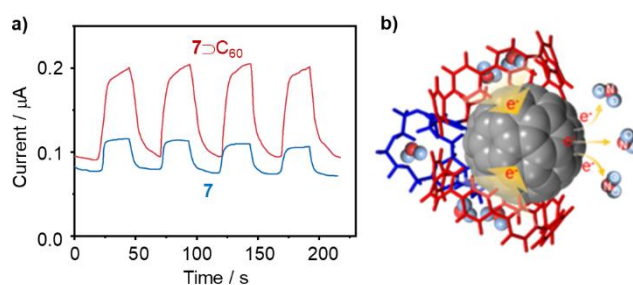


Fig. 6 | a) Photocurrent of the $7\supset C_{60}$ complex and **7** at 5 V. b) The proposed sensing mechanism of $7\supset C_{60}$ for NO_2 .

To further understand the significantly enhanced gas-sensing response of the $7\supset C_{60}$ complex compared to **7**, we first tested the transient photocurrent of both devices in air (Fig. 6a). The results revealed that the $7\supset C_{60}$ complex exhibited a higher current intensity under simulated sunlight compared to **7**, indicating that photo-generated charge carriers in the $7\supset C_{60}$ complex are more easily separated and directed for transport. This provides further evidence of a distinct D-A effect in the $7\supset C_{60}$ complex. As shown in Fig. 6b, during the NO_2 detection process, **7** effectively captures and concentrates NO_2 molecules. Due to the D-A structure, the charge transfer barrier between the **7** and NO_2 is disrupted by C_{60} . As an electron transport mediator, C_{60} facilitates efficient electron transfer to NO_2 , leading to a significant decrease in the electron density on the $7\supset C_{60}$ complex. This, in turn, increases the resistance and enhances the gas-sensing response. Upon removal of NO_2 from the $7\supset C_{60}$ complex, the electrons released by NO_2 return to the complex, restoring the sensor's resistance to its baseline state. Moreover, the D-A structure ensures the directional transport of electrons, thereby enabling stable responses to NO_2 detection.

Biological Application Evaluation. Incorporating polar side-chain functionalization into the CPP ring may enhance the macrocycles' utility in biosensing and bioimaging applications.²⁰ Cell imaging and in vitro antitumor activity studies were performed to evaluate the biological potential of the bismacrocycle **5**. Fluorescence imaging with the HeLa cervical cancer cell line

was conducted to assess the bismacrocycle's cellular uptake. After 90 minutes of incubation, weak green fluorescence was observed within the cells, indicating successful penetration of the cell membrane (Fig. 7a, A–C). Lipopolysaccharide (LPS), a well-known inflammatory stimulus, induces reactive oxygen species (ROS) production in cells, increasing cytoplasmic viscosity and promoting inflammation.²¹ When cells were pretreated with LPS (1 µg/mL) for 30 minutes before exposure to the bismacrocycle **5**, a marked increase in fluorescence intensity was observed (Fig. 7a, D and E). This enhancement was significantly greater than that in the control group (Fig. 7b), suggesting the bismacrocycle's potential for identifying and distinguishing inflammatory cells. The observed increase in fluorescence after LPS pretreatment may be attributed to changes in cellular viscosity, which could facilitate the radiative transition of the compound in inflammatory cells.²² This finding is important, as it highlights the bismacrocycle's ability to detect and monitor inflammatory responses within cells.

Next, the cytotoxicity of the compound was evaluated in HeLa, H520 (lung cancer), and BEAS-2B (normal lung epithelial) cells using the MTT assay. As shown in Fig. 7c, the bismacrocycle **5** exhibited significant cytotoxicity across all cell lines at a minimal concentration of 3 µM after 24 hours of incubation. The half-maximal inhibitory concentration (IC₅₀) values for HeLa, H520, and BEAS-2B cells were determined to be 3.700, 2.813, and 2.778 µM, respectively (Fig. 7d). These relatively low IC₅₀ values underscore the bismacrocycle's potent antitumor activity, which has not been previously reported in the literature.

The bismacrocycle's potent cytotoxicity at low concentrations, with IC₅₀ values notably lower than those of comparable nanohoops, suggests a superior therapeutic index and emphasizes its potential as an effective anticancer agent. This is particularly significant given the growing demand for drugs with high potency. Collectively, these findings lay a strong foundation for advancing the compound as a novel imaging agent and anticancer therapeutic, with promising applications in the imaging and treatment of various cancer types.

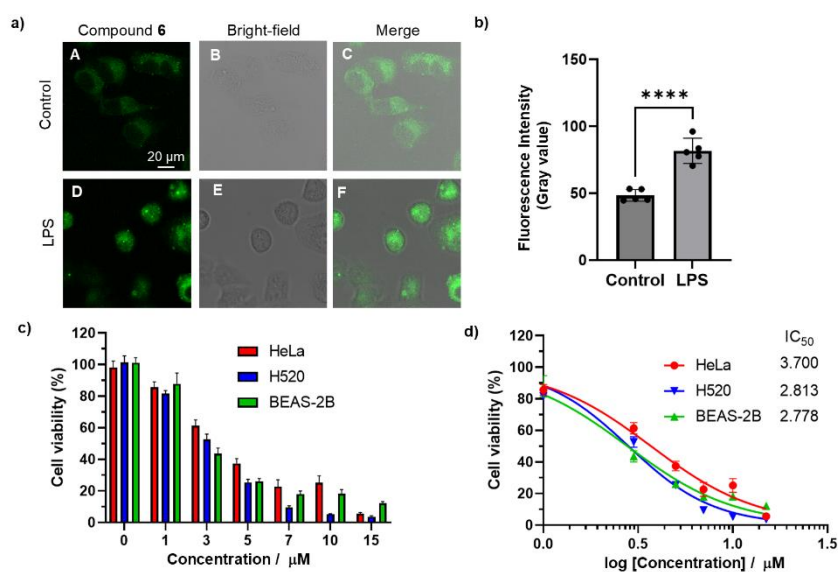


Fig. 7 | a) Confocal fluorescence imaging of HeLa cells. Control groups (A–C): the cells were incubated with **5** for 90 minutes. LPS groups (D and E): The cells were pretreated with LPS (1 μg/mL) for 30 minutes before incubating with **5**. $\lambda_{\text{ex}} = 405$ nm, $\lambda_{\text{em}} = 500\text{--}600$ nm. b) Comparison of the fluorescence intensity of the cells in (A) and (D). Data are expressed as the Mean \pm SD, n = 5. Statistical significance is denoted by **** (p < 0.0001). c) Cell viability and (d) inhibition rates of HeLa, H520, and BEAS-2b cells with different concentrations of the Compound (0, 1, 3, 5, 7, 10, and 15 μM). Data are expressed as Mean \pm SD, n = 3.

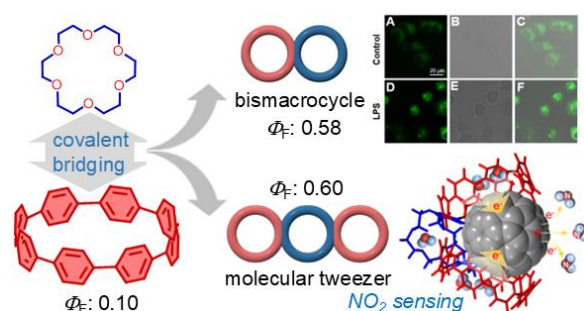
Conclusion

In this study, we have successfully designed and synthesized a series of crown ether- CPP hybrid multimacrocycles and explored their supramolecular properties, photophysical behavior, and biological applications. The integration of crown ethers into the CPP framework not only improves solubility and enhances fluorescence quantum yield but also introduces new binding sites that facilitate selective host-guest interactions. Notably, the trimacrocyclic hybrid adopts a molecular tweezer-like conformation, leading to a five-fold increase in fullerene binding affinity compared to its bismacrocyclic counterpart. This enhanced host-guest recognition behavior, supported by fluorescence quenching titrations and density functional theory (DFT) calculations, provides new insights into the design of high-affinity supramolecular receptors. Additionally, the fullerene complex was explored as a chemiresistive gas sensor for NO₂ detection. It showed improved conductivity and sensitivity with a LOD of 19 ppb, thanks to its D-A structure and fullerene's role as an electron transport mediator. The sensor also demonstrated excellent cyclic stability and reliable, directional electron transport for NO₂ detection.

The biological evaluation of these hybrid macrocycles further underscores their potential for

biomedical applications. The bismacrocycle exhibits significant cytotoxicity against cancer cell lines at micromolar concentrations, with IC_{50} values lower than those of comparable nano hoops, highlighting its promise as a novel anticancer agent. Moreover, its fluorescence-based detection of inflammatory responses suggests potential applications in biosensing and imaging. These findings collectively demonstrate that crown ether-CPP hybrids represent a new class of multifunctional macrocycles with broad applicability in supramolecular sensing²³ and biochemistry²⁴.

TOC:



Data availability

General experimental details and procedures, X-ray crystallographic details, computational details, 1H NMR spectra, $^{13}C\{^1H\}$ NMR spectra, and others data generated in this study are available within the article Supplementary Information. The X-ray crystallographic coordinates for structures reported in this study have been deposited at the Cambridge Crystallographic Data Centre (CCDC), under deposition numbers CCDC 2393490 for **6** and 2393489 for **and6** $\supset K^+$. These data can be obtained free of charge from The Cambridge Crystallographic Data Centre via www.ccdc.cam.ac.uk/data_request/cif.

References:

- (a) Ogoshi, T., Yamagishi, T.A. & Nakamoto, Y. Pillar-shaped macrocyclic hosts pillar[n]arenes: New key players for supramolecular chemistry. *Chem. Rev.* **116**, 7937–8002 (2016). (b) Chang, X. Xu, Y. & M. von Delius. Recent advances in supramolecular fullerene chemistry. *Chem. Soc. Rev.* **53**, 47–83 (2024). (c) Long, Y.-J., Han, X.-N., Han, Y. & C.-F. Chen. Recent advances in supramolecular luminescent materials based on macrocyclic arenes. *Chin. Chem. Lett.* DOI: 10.1016/j.ccl.2024.110600 (2025). (d) Yu, Y., Hu, Y., Ning, C., Shi, W., Yang, A., Zhao, Y., Cao, Z.-Y., Xu, Y. & Du, P. BINOL-based chiral macrocycles and cages. *Angew. Chem. Int. Ed.* **63**, e202407034 (2024).
- (a) Clayton, T. D., Fehr, J. M., Price, T. W., Zakharov, L. N. & Jasti, R. Pinwheel-like curved

- aromatics from the cyclotrimerization of strained alkyne cycloparaphenylenes. *J. Am. Chem. Soc.* **146**, 30607–30614 (2024). (b) Xu, Y., Leung, M.-Y., Yan, L., Chen, Z., Li, P., Cheng, Y.-H., Chan, M. H.-Y. & Yam, V. W.-W. Synthesis, characterization, and resistive memory behaviors of highly strained cyclometalated platinum(II) nanohoops. *J. Am. Chem. Soc.* **146**, 13226–13235 (2024). (c) Shi, W., Zhao, Y. & Xu, Y. Strain-promoted reactivity in carbon nanohoops. *Trends Chem.* **7**, 1–2 (2025).
3. Darzi, E. R. & Jasti, R. The dynamic, size-dependent properties of [5]-[12]cycloparaphenylenes. *Chem. Soc. Rev.* **44**, 6401–6410 (2015).
4. (a) Li, Y., Kono, H., Maekawa, T., Segawa, Y., Yagi, A. & Itami, K. Chemical synthesis of carbon nanorings and nanobelts. *Acc. Mater. Res.* **2**, 681–691 (2021). (b) Malinčík, J., Gaikwad, S., Mora-Fuentes, J. P., Boillat, M.-A., Prescimone, A., Häussinger, D., Campaña, A. G. & Šolomek, T. Circularly polarized luminescence in a möbius helicene carbon. *Angew. Chem. Int. Ed.* **61**, e202208591 (2022). (c) Hermann, M., Wassy, D. & Esser, B. Conjugated nanohoops incorporating donor, acceptor, hetero- or polycyclic aromatics. *Angew. Chem. Int. Ed.* **60**, 15743–15766 (2021). (4) Stergiou, A., Rio, J., Griwatz, J. H., Arcon, D., Wegner, H. A., Ewels, C. & Tagmatarchis, N. A long-lived azafullerenyl radical stabilized by supramolecular shielding with a [10]cycloparaphenylene. *Angew. Chem. Int. Ed.* **58**, 17745–17750 (2019).
5. (a) Chen, X.-L., Yu, S.-Q., Huang, X.-H. & Gong, H.-Y. Bismacrocycle: Structures and applications. *Molecules* **28**, 6043 (2023). (b) Zhang, Y., Yang, D., Pun, S. H., Chen, H. & Miao, Q. Merging a negatively curved nanographene and a carbon nanoring. *Precis. Chem.* **1**, 107–111 (2023). (c) He, J., Yu, M.-H., Lian, Z., Fan, Y.-Q., Guo, S.-Z., Li, X.-N., Wang, Y., Wang, W.-G., Cheng, Z.-Y. & Jiang, H. Lemniscular carbon nanohoops with contiguous conjugation from planar chiral [2.2]paracyclophane: influence of the regioselective synthesis on topological chirality. *Chem. Sci.* **14**, 4426 (2023). (d) Zhang, X., Xu, Y. & P. Du. Functional bis/multi-macrocylic materials based on cycloparaphenylene carbon nanorings. *Acc. Mater. Res.* **6**, 399–410 (2025). (e) Li, G., Mao, L.-L., Gao, J.-N., Shi, X., Huo, Z.-Y., Yang, J., Zhou, W., Li, H., Yang, H.-B., Tung, C.-H., Wu, L.-Z. & Cong, H. A helical tubular dyad of [9]cycloparaphenylene: Synthesis, chiroptical properties and post-functionalization. *Angew. Chem. Int. Ed.* **64**, e202419435 (2025). (f) Yang, Y., Blacque, O., Sato, S. & Juríček, M. Cycloparaphenylene–phenalenyl radical and its dimeric double nanohoop. *Angew. Chem. Int. Ed.* **60**, 13529–13535 (2021). (g) Ren, L., Han, Y., Hou, X., Zou, Y., Jiao, T. & Wu, J. Cyclooctatetrathiophene annulated multicyclic macrocycles. *CCS Chem.* **6**, 2758–2769 (2024). (h) Chen, X.-W., Deng, Q.-S., Zheng, B.-H., Xing, J.-F., Pan, H.-R., Zhao, X.-J. & Tan, Y.-Z. Cylindrical and conical conjugated nanobelts by longitudinal extension of

- cycloparaphenylene and their double-walled assembly. *J. Am. Chem. Soc.* **146**, 31665–31670 (2024). (i) Li, K.; Yoshida, S.; Yakushiji, R., Liu, X., Ge, C., Xu, Z., Ni, Y., Ma, X., Wu, J., Sato, S. & Sun, Z. Molecular cylinders with donor–acceptor structure and swinging motion. *Chem. Sci.* **15**, 18832–18839 (2024). (j) Liu, Y., Lei, P., Feng, Y., Fu, S., Liu, X., Zhang, S., Tu, B., Chen, C., Li, Y., Wang, L. & Zeng, Q.-D. Topologically engineering of π -conjugated macrocycles: Tunable emission and photochemical reaction toward multi-cyclic polymers. *Chin. Chem. Lett.* **35**, 109571 (2024). (k) Senthilkumar, K., Kondratowicz, M., Lis, T., Chmielewski, P. J., Cybinska, J., Zafra, J. L., Casado, J., Vives, T., Crassous, J., Favereau, L., Stępień, M. Lemniscular [16]cycloparaphenylene: A radially conjugated figure-eight aromatic molecule. *J. Am. Chem. Soc.* **141**, 7421–7427 (2019).
6. Zhang, X., Liu, H., Zhuang, G., Yang, S. & Du, P. An unexpected dual-emissive luminogen with tunable aggregation-induced emission and enhanced chiroptical property. *Nat. Commun.* **13**, 3543 (2022).
7. (a) Xu, Y., Steudel, F., Leung, M., Xia, B., von Delius, M. & Yam, V. W-W. [n]Cycloparaphenylene-pillar[5]arene bismacrocycles: Their circularly polarized luminescence and multiple guest recognition properties. *Angew. Chem. Int. Ed.* **62**, e202302978 (2023). (b) Fan, Y., Fan, S., Liu, L., Guo, S., He, J., Li, X., Lian, Z., Guo, W., Chen, X., Wang, Y. & Jiang, H. Efficient manipulation of Förster resonance energy transfer through host–guest interaction enables tunable white-light emission and devices in heterotopic bisnanohoops. *Chem. Sci.* **14**, 11121–11130 (2023). (c) Zhou, Y., Zhuang, G. & Du, P. Selective synthesis and physical properties of a bismacrocyclic cycloparaphenylene-pillar[5]arene. *Chin. Chem. Lett.* **35**, 108593 (2024).
8. (a) Lewis, J. E. M., Beer, P. D., Loeb, S. J., Goldup, S. M. Metal ions in the synthesis of interlocked molecules and materials. *Chem. Soc. Rev.* **46**, 2577–2591 (2017). (b) Chen, L., Sheng, X., Li, G. & Huang, F. Mechanically interlocked polymers based on rotaxanes. *Chem. Soc. Rev.* **51**, 7046–7065 (2022). (c) Evans, N. H. & Beer, P. D. Progress in the synthesis and exploitation of catenanes since the Millennium. *Chem. Soc. Rev.* **43**, 4658–4683 (2014). (d) Goswami, A., Saha, S., Biswas, P. K. & Schmittel, M. (Nano)mechanical motion triggered by metal coordination: from functional devices to networked multicomponent catalytic machinery. *Chem. Rev.* **120**, 125–199 (2019).
9. Shi, W., Hu, Y., Leanza, L., Shchukin, Y., Hoffmann, P. A., Li, M., Ning, C., Cao, Z.-Y., Xu, Y.-Q., Du, P., von Delius, M., Pavan, G. M. & Xu, Y. Ring-in-ring assembly facilitates the synthesis of a [12]cycloparaphenylene ABC-type [3]catenane. *Angew. Chem. Int. Ed.* **64**, e202421459 (2025).
10. Zhong, H., Lan, K., Ming, J., Zhang, D. & Cheng, C. Stereoisomerism in trimacrocyclic

- structures fused by a pillar[6]arene and two [8]cycloparaphenylenes. *Org. Lett.*, **27**, 4349–4354 (2025).
11. Xia, J., Bacon, J. W. & Jasti, R. Gram-scale synthesis and crystal structures of [8]- and [10]CPP, and the solid-state structure of C₆₀@[10]CPP. *Chem. Sci.* **3**, 3018–3021 (2012).
 12. Lovell, T. C., Colwell, C. E., Zakharov, L. N. & Jasti, R. *Chem. Sci.* **10**, 3786–3790 (2019).
 13. (a) Xu, Y. & von Delius, M. The supramolecular chemistry of strained carbon nanohoops. *Angew. Chem. Int. Ed.* **59**, 559–573 (2020). (b) García-Simón, C., Costas, M. & Ribas, X. Metallo-supramolecular receptors for fullerene binding and release. *Chem. Soc. Rev.* **45**, 40–62 (2016).
 14. Iwamoto, T., Watanabe, Y., Sadahiro, T., Haino, T., Yamago, S. Size-selective encapsulation of C₆₀ by [10]cycloparaphenylene: Formation of the shortest fullerene-peapod. *Angew. Chem. Int. Ed.* **50**, 8342–8344 (2011).
 15. (a) Sacristan-Martin, A., Barbero, H., Ferrero, S., Miguel, D., Garcia-Rodriguez, R. & Alvarez, C. M. ON/OFF metal-triggered molecular tweezers for fullerene recognition. *Chem. Commun.* **57**, 11013–11016 (2021). (b) Scholz, B., Oshchepkov, A. S., Papaianina, O., Ruppenstein, C., Akhmetov, V. A., Sharapa, D. I., Amsharov, K. Y. & Pérez-Ojeda, M. E. *Chem. – Eur. J.* **29**, e202302778 (2023). (c) Mirzaei, M. S., Mirzaei, S., Castro, V. M. E., Lawrence, C. & Sánchez, R. H. *Chem. Commun.* **60**, 14236–14239 (2024).
 16. <http://supramolecular.org>
 17. Zhang, Y., Liu, Q., Sun, Q., Li, H., Shen, J., Liu, H., Chen, W., Zhang, Y. & Chen, Y. Metalloporphyrin-based metal–organic frameworks for the ultrasensitive chemiresistive detection of NO₂: Effect of the central metal on tuning the sensing performance. *ACS Sens.* **8**, 4353–4363 (2023).
 18. Liu, Q., Li, Q., Li, Y., Su, T., Hou, B., Zhao, Y. & Xu, Y. Two-dimensional covalent organic frameworks in organic electronics. *Angew. Chem. Int. Ed.* **64**, e202502536 (2025).
 19. (a) Liu, Q., Sun, Q., Li, H., Zhang, Y., Feng, L., Chen, W. & Chen, Y. Self-adaptable porphyrin-phthalocyanine-based conjugated polymer nanozyme for intelligent biosensing. *Sens, Actuators B: Chem.* **428**, 137250 (2025). (b) Ding, K., Zhang, K., Liu, X., Xu, Q., Cheng, X., Yao, M., Wang, W., Zeng, Y., Ye, T., He, Y., Lin, W., Zhou, R., Chen, Ya. & Li, S. *ACS Nano* **19**, 8238–8254 (2025).
 20. (a) Günther, K., Kono, H., Shudo, H., Shimizu, D., Isoda, R., Nakamura, M., Yagi, A., Amaike, K. & Itami, K. Water-doluble aromatic nanobelt with unique cellular internalization. *Angew. Chem. Int. Ed.* **64**, e202414645 (2025). (b) White, B. M., Zhao, Y., Kawashima, T. E., Branchaud, B. P., Pluth, M. D., Jasti, R. Expanding the chemical space of biocompatible fluorophores: Nanohoops in cells. *ACS Cent. Sci.* **4**, 1173–1178 (2018).

21. (a) Zhang, Y., Li, Z., Hu, W. & Liu, Z. A mitochondrial-targeting near-infrared fluorescent probe for visualizing and monitoring viscosity in live cells and tissues. *Anal. Chem.* **91**, 10302–10309 (2019). (b) Li, Y.-Y., Hu, J.-L., Wu, J.-R., Wang, Y.-R., Zhang, A.-H., Tan, Y.-W., Shang, Y.-J., Liang, T., Li, M., Meng, Y.-L. & Kang, Y.-F. *Biosens. Bioelectron.* **254**, 116233 (2024).
22. (a) Feng, S., Gong, S., Zheng, Z. & Feng, G. *Sensor. Actuat. B-Chem.* **351**, 130940 (2022). (b) Wu, W.-N., Song, Y.-F., Zhao, X.-L., Wang, Y., Fan, Y.-C., Xu, Z.-H. & James, T. D. Multifunctional 1,3-benzoxazole-merocyanine-based probe for the ratiometric fluorescence detection of pH/HSO₃⁻/viscosity in mitochondria. *Chem. Eng. J.* **464**, 142553 (2023).
23. (a) Chen, Q. & Zhu, K. Advancements and strategic approaches in catenane synthesis. *Chem. Soc. Rev.* **53**, 5677–5703 (2024). (b) Zhang, Z., Zhao, J. & Yan, X. Mechanically interlocked polymers with dense mechanical bonds. *Acc. Chem. Res.* **57**, 992–1006 (2024). (c) C. Wang, L. Xu, Z. Jia and T.-P. Loh, *Chin. Chem. Lett.*, 2024, **35**, 109075. (d) Regehly, M., Garmshausen, Y., Reuter, M., König, N. F., Israel, E., Kelly, D. P., Chou, C.-Y., Koch, K., Asfari, B. & Hecht, S. *Nature* **588**, 620–624 (2020). e) Tang, Z.-B., Bian, L., Miao, X., Gao, H., Liu, L., Jiang, Q., Shen, D., Xu, L., Sue, A. C.-H., Zheng, X. & Liu, Z. Synthesis of a crystalline two-dimensional [c2]daisy chain honeycomb network. *Nat. Synth.* 2025, DOI: 10.1038/s44160-025-00791-x.
24. Chinner, K., Grabicki, N., Hamaguchi, R., Ikeguchi, M., Kinbara, K., Toyoda, S., Sato, K. & Dumele, O. Nanohoops in membranes: confined supramolecular spaces within phospholipid bilayer membranes. *Chem. Sci.* **15**, 16367–16376 (2024).

Acknowledgements

We acknowledge funding from the National Natural Science Foundation of China (22471060 and 22201064), the Joint Fund of Henan Provincial Science and Technology Research and Development Plan (235200810074) and the Key Scientific Research Project of Colleges and Universities in Henan Province (24A330005).

Author contributions

Y.X. proposed the concept. Y.H. led the synthesis of the compounds, conducted the characterizations, and analyzed the data. Q.L. prepared the electronic devices and performed the sensing experiments. T.L. and D.W. carried out cell imaging and in vitro antitumor activity studies. Y.X., Q.L., and D.W. wrote the manuscript. All authors contributed to the discussions and revisions of the manuscript.